Plasma-enhanced catalytic activation of CO_2 in a modified gliding arc reactor

Hao Zhang[1], Li Li[1], Ruiyang Xu[1], Jingying Huang[1], Ni Wang[2], Xiaodong Li[1*], Xin Tu[2*]

[1] State Key Laboratory of Clean Energy Utilization, Zhejiang University, Hangzhou, 310027, China.
[2] Department of Electrical Engineering and Electronics, University of Liverpool, Liverpool L69 3GJ, UK.

Corresponding authors

Prof. Xiaodong Li (lixd@zju.edu.cn), Prof. Xin Tu (xin.tu@liverpool.ac.uk)

Abstract:

For the first time, this paper demonstrates a synergistic effect from the combination of a gliding arc discharge plasma with a photocatalyst TiO_2 for CO_2 dissociation. The effects of adding a tray downstream the discharge and the combination of catalyst with plasma have been investigated. Two different combination modes of plasma catalysis, *i.e.*, in-plasma catalysis and post-plasma catalysis, have been evaluated with the emphasis on the analysis of potential mechanisms. The results show that modifying the gliding arc reactor by the addition of a tray can enhance the fraction of gas treated by plasma, thus improving the reaction performance. An exceptional synergistic effect of combining the gliding arc discharge with TiO_2 for CO_2 activation forms in the in-plasma catalysis mode. The presence of TiO_2 significantly enhances the CO_2 conversion by 138% and the energy efficiency by 133% at a flow rate of 2 L/min. The plasma activation effect, which produces energetic electrons that can create the electron-hole pairs on the catalyst surface, is believed to be the major contributor to the generation of the plasma catalysis synergy. This mechanism has been further evidenced by the negligible influence of the post-plasma catalysis on the reaction performance.

Keywords: CO_2 activation; Plasma catalysis; TiO_2; Synergistic effect

1. Introduction

Accumulating evidence has demonstrated that the increasing greenhouse gases emission caused by human activities is leading to global climate change [1]. As a major greenhouse gas, CO_2 contributes 85% to the overall global warming [2]. The levels of CO_2 in the atmosphere have dramatically increased from 280 ppm in the pre-industrial era to a historical high of 408 ppm (July 2018 [3]). Undoubtedly, there is an unprecedented need to develop low carbon technologies to mitigate and valorize CO_2. Carbon capture and utilization (CCU) is one of the most attractive strategies as it can convert CO_2 into value-added fuels and chemicals [4-6]. In this regard, several chemical processes have been extensively studied, such as dry reforming and hydrogenation of CO_2, producing value-added syngas or oxygenates [6, 7]. CO_2 splitting to CO is of particular interest (Eq. (1)) as well [6, 8-11] as CO is a commonly used feedstock for the synthesis of platform chemicals (e.g., organic acids, aldehydes and alcohols) and synthetic fuels [12]. However, due to the inherent kinetic inertness of CO_2, its activation remains a big challenge. Thermal CO_2 dissociation is energetically favourable only at high temperatures. For instance, only up to 1.5% of CO_2 conversion can be achieved at a temperature of 2000 K, yielding an energy efficiency of 4.4% [6].

$$CO_2 \rightarrow CO + \frac{1}{2}O_2 \qquad \Delta H = 280 \text{ kJ/mol} \tag{1}$$

Recently, non-thermal plasma technology has attracted significant interest in CO_2 dissociation since it can activate CO_2 at atmospheric pressure and low temperatures with reduced energy consumption [6, 13, 14]. The electrons in non-thermal plasma have average electron energy of 1-10 eV, which is high enough to activate CO_2 molecules, producing a cascade of radicals, excited molecules/atoms, and ions etc. These species are highly reactive and play a key role in plasma chemical

reactions [15-18]. However, because of the non-equilibrium character of non-thermal plasma, the gas kinetic temperature can remain fairly low (*e.g.*, 200-800 ^{o}C), thus saving energy [19, 20]. Moreover, due to the merits of high specific productivity and instant on/off, non-thermal plasma system is a promising technology to utilize excess intermittent renewable energy, such as wind and solar power, for energy storage [11].

Various non-thermal plasma sources have been studied for the dissociation of CO_2, including dielectric barrier discharge (DBD) [9-11, 13, 21-27], microwave (MW) discharge [4, 7, 28, 29], corona discharge [30, 31] and gliding arc discharge [5, 32-35]. In non-thermal plasmas, the electron-impact dissociation of CO_2 can proceed only with an electron energy of > 7 eV to activate CO_2 molecule to a dissociative electronic state. However, the amount of energy spent is significantly higher than the theoretical energy needed for C=O bond breaking (5.5 eV), thus resulting in energy waste. Vibrational excitation of CO_2 is considered as the most effective means for CO_2 activation because it requires the least amount of energy [15, 28, 35]. The non-adiabatic transition $o\,^1\Sigma^+ \rightarrow {}^3B_2$ pens the most effective dissociation pathway of CO_2 with an energy requirement of only 5.5 eV [28]. In DBD and corona discharge, the electron-impact excitation predominates in the dissociation of CO_2, leading to fairly low energy efficiency (typically <15%) [6, 27, 30]. MW discharge allows for a high level of CO_2 vibrational excitation and thus show a relatively high energy efficiency (up to 40% [28]). However, this is achievable only at low pressure (e.g., 50 torrs) [36], which is unfavourable for industrial applications. Note that the energy efficiency reported in these works typically only considers the power deposit in the MW plasma but does not consider the extra power consumed of the vacuum systems [36].

Atmospheric pressure gliding arc plasma is becoming increasingly attractive for CO_2 activation

as the high level of CO_2 vibrational excitation in this process enables more effective activation of CO_2 [6, 35]. A moderate electron temperature of gliding arc, *i.e.*, 1-2 eV, is ideal for full exploitation of the vibrational excitation of CO_2 [5, 17, 36, 37]. Moreover, the electron density of gliding arc discharges is remarkably higher compared with other non-thermal plasmas (*e.g.*, corona discharge and DBD), which is favourable for industrial applications due to its flexibility to operate at variable conditions [15, 38]. A traditional gliding arc reactor consists of two or more diverging electrodes (for the generation of arc) and a gas nozzle (for injecting the carrier gas) [38]. After initiation at the shortest electrode gap, the arc is pushed by the gas stream toward the diverging downstream section, until it extinguishes. A new period then starts with the formation of a new arc at the shortest gap. However, the 2D geometry of the gliding arc limits gas conversion as only a small part of the reactant can pass through the plasma zone (*e.g.*, about 20% depending on the geometry [5, 6]). In addition, a high flow rate is required to sustain the arc, which limits the residence time inside the plasma. However, limited works have been done to optimize the gas flow field in the gliding arc reactor, which is necessary to enhance the plasma gas conversion.

In recent years, particular attention has been paid to plasma catalysis, *i.e.*, the integration of plasma with catalysts for environmental clean-up, fuel reforming and chemical synthesis [39, 40]. The combination of plasma and catalyst provides significant potential to produce a synergy effect to increase the reaction rate by reducing the activation barrier of the plasma chemical reactions, consequently increasing the conversion of reactant and selectivity of desired products significantly, and decreasing the energy consumption of the processes [14, 40]. To date, a few works have investigated plasma-catalytic CO_2 dissociation in non-thermal plasmas, including DBD [14, 23] and MW plasmas [4, 7, 29, 41]. For instance, Mei and Tu reported that the combination of Ni/γ-Al_2O_3 with

a DBD improved both the conversion of CO_2 and the energy efficiency in comparison to the γ-Al_2O_3 support, from 24.7% to 26.3% and 3.9% to 4.1% [23]. However, performance is still not competitive.

To the best of our knowledge, the integration of catalysis with plasma for CO_2 activation using gliding arc discharges has not been reported. In this work, the plasma catalytic dissociation of CO_2 over a photocatalyst (TiO_2) has been investigated for the first time in a modified gliding arc discharge [4, 14]. In addition, a round tray (with different diameters) was placed downstream of the GAD with the dual objectives of optimizing the gas flow field and serving as the catalyst container. The influence of the tray size and the positions of catalysts on the reaction performance have been studied in terms of the CO_2 conversion and energy efficiency. Particular efforts have been devoted to investigating different plasma catalysis modes, *i.e.*, in-plasma catalysis (IPC) and post-plasma catalysis (PPC). In addition, the possible mechanism of plasma catalysis in CO_2 activation has been discussed.

2. Methods

Experimental setup. The reactant gas CO_2 was injected into the homemade gliding arc discharge reactor by a mass flow controller. A high-voltage DC power supply (10 kV, TLP2040, Teslaman) was used to power the plasma, and a resistor of 40 kΩ was used in the circuit to limit and stabilize the discharge current. An on-line gas analyzer (Mamos, Madur electronics) equipped with a CO_2 IR sensor, a CO IR sensor and an O_2 electrochemical sensor was employed to measure the on-line concentrations of CO_2, CO and O_2 before and after the plasma reaction.

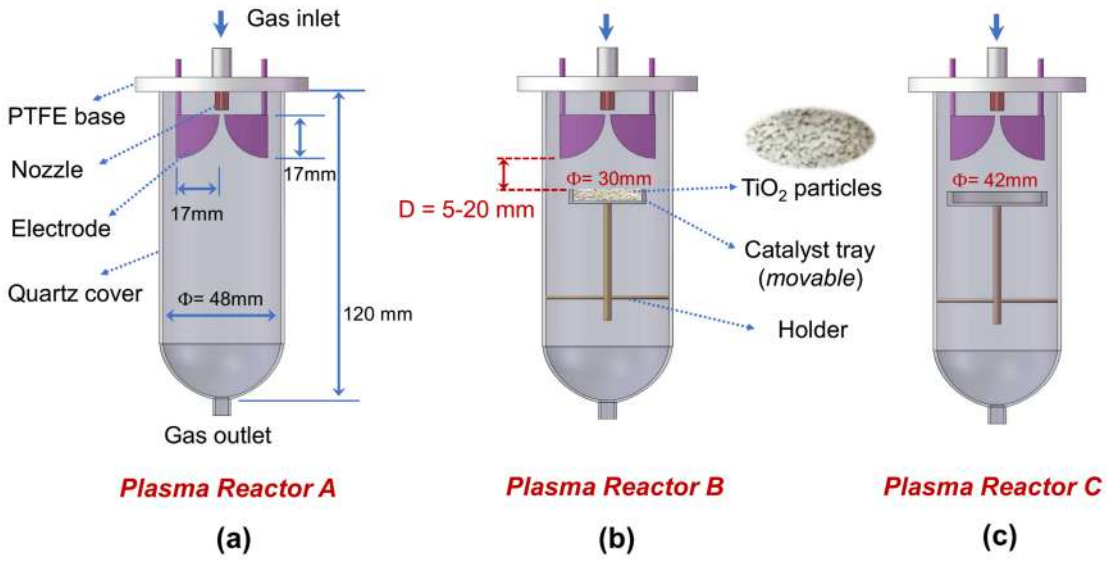

Fig. 1 Configurations of the gliding arc reactors.

Fig. 1 shows the configurations of the reactors used in this work. Each reactor consists of two divergent knife-shaped electrodes (stainless steel, 17 mm in both length and width) with a gas nozzle (with an inner diameter of 1.5 mm) placed upstream. When the applied voltage on the electrodes is high enough for breakdown, the arc forms initially at the shortest gap point (2 mm). The formed arc then glides downstream along the electrodes with increasing length under the force of gas flow until it extinguishes. In *Reactor B* and *Reactor C*, a round tray with a diameter (Φ) of 30 mm and 42 mm, respectively, is placed downstream of the discharge to modify the gas flow field and improve the fraction of gas treated by plasma, and further serve as a catalyst bed. *Reactor B* with the tray of Φ = 30 mm was further investigated in the plasma catalytic conversion of CO_2, with TiO_2 particles as the catalyst. The position of the tray is vertically movable, and the vertical distance between the electrode tip and the tray (D) can be adjusted in the range of 5 to 20 mm. The discharge powers of the gliding arc under the studied conditions are: *Reactor A*: 360±5W; *Reactor B* (D = 10-15 mm, with/without catalyst): 360±10W; *Reactor B* (D = 5 mm, without catalyst): 402±35W; *Reactor B* (D = 5 mm, with

catalyst): 365±11W; *Reactor B* (D = 20 mm, without catalyst): 360±15W; *Reactor B* (D = 20 mm, with catalyst): 343±10W; *Reactor C* (D = 10 mm, without catalyst): 395±35W.

Catalyst material. Commercial photocatalyst TiO_2 (rutile phase) with diameters of 3-5 mm was used as the catalyst. For each plasma catalysis experiment, 3 grams of TiO_2 particles were placed inside the catalyst tray in *Reactor B*, forming a catalyst layer (about 5 mm for each experiment) downstream the discharge. X-ray diffraction (XRD) patterns of the TiO_2 were detected by an XRD-7000 diffractometer (Shimadzu) using radiation in the 2θ range between 10° and 80° at a scanning rate of 4 °/min. The atomic state at the surface of the catalyst was analyzed by X-ray photoelectron spectra (XPS) with Al Ka X-rays (1486.6 eV) on an ESCALAB 250Xi system (Thermo Scientific). The spectra were referenced to C1s peak at 284.5 eV.

Definition of parameters. The CO_2 conversion (X) was defined as follows.

$$X(\mathrm{CO_2})\ (\%)=\frac{Q_{(\mathrm{CO_2\ inlet})}\ (\mathrm{mol/min})\ -\ Q'_{(\mathrm{total\ outlet})}\ (\mathrm{mol/min})\ \times\ C_{(\mathrm{CO_2\ outlet})}\ (\%)}{Q_{(\mathrm{CO_2\ inlet})}\ (\mathrm{mol/min})}\times 100\% \qquad (2)$$

, where $Q_{(\mathrm{CO2\ inlet})}$ and $Q'_{(\mathrm{total\ outlet})}$ is the inlet CO_2 flow rate and outlet total flow rate, respectively, $C_{(\mathrm{CO2\ outlet})}$ is the CO_2 concentration in the outlet effluent gas.

In the CO_2 splitting reaction, two CO_2 molecules are dissociated into three molecules (see Eq. (1)), which increases the volume by 50%. That means the total outlet flow rate should be higher than the inlet flow rate (gas expansion effect) [5, 22], which is directly associated with the accuracy of the calculated CO_2 conversion. However, the gas expansion effect is often neglected by most of the authors, overestimating the CO_2 conversion and energy efficiency (*e.g.*, be overestimated by a factor of 1.5 in case of 100% conversion). In this work, the gas expansion effect has been considered. Our experiments

showed that the selectivity of CO remains at > 99% and the total concentration of CO_2, CO and O_2 in the effluent gas is 100±1% in the experiments, showing that the CO_2 splitting to CO and O2 (Eq. (1)) was dominant in this process. Therefore, the $Q'_{(\text{total outlet})}$ can be obtained according to the carbon balance before and after the reaction, based on the following equation.

$$Q'_{(\text{total outlet})}\ (\text{mol/min}) = \frac{Q_{(CO_2\ \text{inlet})}\ (\text{mol/min})}{C_{(CO_2\ \text{outlet})}\ (\%) + C_{(\text{CO outlet})}\ (\%)} \times 100\% \quad (3)$$

, where $C_{(\text{CO outlet})}$ is the CO concentration in the outlet effluent gas.

The energy efficiency (η) was defined as follows by comparing the energy consumption of the plasma process to the standard reaction enthalpy (ΔH):

$$\eta(\%) = \frac{Q_{(CO_2\ \text{inlet})}\ (\text{mol/min}) \times X(CO_2)\ (\%) \times \Delta H(\text{kJ/mol})}{\text{Discharge power (W)} \times 60/1000} \quad (4)$$

, where ΔH = 280 kJ/mol for the CO_2 dissociation process. The discharge power was determined by the product of the arc voltage and arc current.

In this work, each experiment was repeated three times, and the mean values with error bars were given in the figures.

3. Results

3.1 Effect of the addition of tray in the reactor

To investigate the effect of tray addition (with different diameters) on the reaction performance, three

types of gliding arc reactors were used in this work, *i.e.*, *Reactor A* without tray, *Reactor B* with tray of 30 mm in diameter (Φ) and *Reactor C* with tray of Φ = 42 mm (see Fig. 1). The results are illustrated in Fig. 2, upon rising CO_2 feed flow rate. Clearly, for each case, the CO_2 conversion first increases to a maximum value and then drops remarkably with increasing flow rate. It should be noted that most of the previous studies in DBD [11, 13, 21] and gliding arc plasmatron [5] showed a monotonous decrease in CO_2 conversion when the CO_2 flow rate increased, resulting from the decreased retention time of CO_2 in plasma and the reduced specific energy input (SEI). In the gliding arc discharge, the gas temperature is relatively high (*e.g.*, up to 2000K, depending on the radial distance [10]), which can enhance the recombination reaction of CO and O (with rate constant of up to 8.0×10^{-34} $cm^6/molecule^2\cdot s$ [42]), thus inhibiting the conversion of CO_2 [12]. The enhancement of CO_2 conversion with the initial increase of CO_2 flow rate might result from the weakening of the recombination of CO and O with decreased gas temperature, as partly demonstrated by the temperature measurement in Supplementary Table S1. For example, the gas temperature of *Reactor B* in the tail of the discharge (at the tray) decreased from 720 to 440 °C, yielding a CO + O recombination rate constant of from 3.7×10^{-34} to 2.0×10^{-34} $cm^6/molecule^2\cdot s$ [42]. Note that the reaction rate in the central arc discharge area should be even higher due to the significantly higher gas temperature. After reaching the maximum value, the further drop of CO_2 conversion with a rising flow rate could be related to the decrease in both the retention time of CO_2 and the SEI. For instance, for *Reactor A*, the retention time of CO_2 and the SEI dropped from 127.5 to 36.4 ms and 10.9 to 3.0 kJ/L, respectively, when the flow rate increased from 2 to 7 L/min. Note that the retention time of CO_2 (the volume of plasma divided by volumetric gas flow rate) is only a roughly calculated value, and the plasma volume is assumed to be around 4.25 cm^3 based on the photographs of the discharge in the experiments. In agreement with other studies [23, 30],

increasing CO_2 flow rate significantly enhances the energy efficiency.

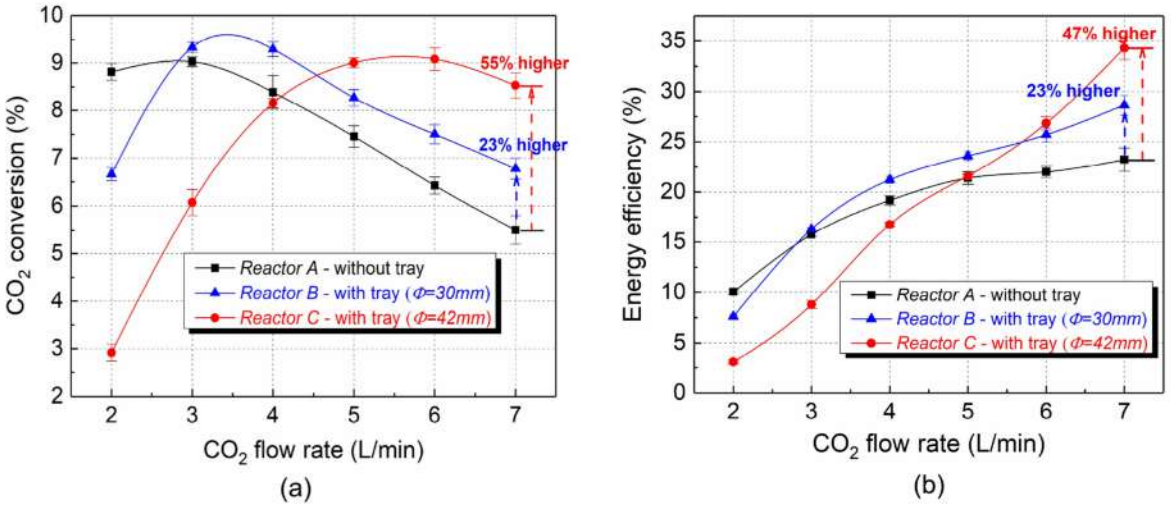

Fig. 2 a) CO_2 conversion and b) energy efficiency as a function of CO_2 flow rate in the three types of reactors with or without tray (D = 10 mm).

Fig. 2 indicates that the addition of tray downstream the plasma can significantly influence the CO_2 dissociation performance in the gliding arc reactor. *Reactor B* with a small tray of Φ = 30 mm and *Reactor C* with a big tray of Φ = 42 mm can both improve the CO_2 conversion and energy efficiency pronouncedly, majorly at a relatively high flow rate of > 4 L/min. The big tray exhibits a significantly higher CO_2 conversion in comparison to the small tray when the flow rate is over 5 L/min. For instance, at a flow rate of 7 L/min, the CO_2 conversion is enhanced by 23% and 55%, respectively, and the energy efficiency is improved by up to 23% and 47%, respectively, in *Reactor B* and *C*. Another phenomenon that needs to be noted is that a relatively low flow rate in *Reactor B* and *C* (especially *Reactor C*) gives a lower CO_2 conversion and energy efficiency in comparison to the *Reactor A* without tray. In addition, the flow rate value for the maximum CO_2 conversion in Fig. 2a is shifted backward

from 3 L/min to 3.5 L/min and 5.5 L/min, respectively, in *Reactor B* and *C*. This phenomenon is probably associated with the increased gas temperature of the plasma area (especially at relatively low flow rates, see Supplementary Table S1) because of the reduced heat loss under the sealing effect of the tray. As mentioned above, a higher gas temperature in the gliding arc is probably detrimental to the CO_2 conversion. Note that further plasma modelling study is still needed to confirm this hypothesis.

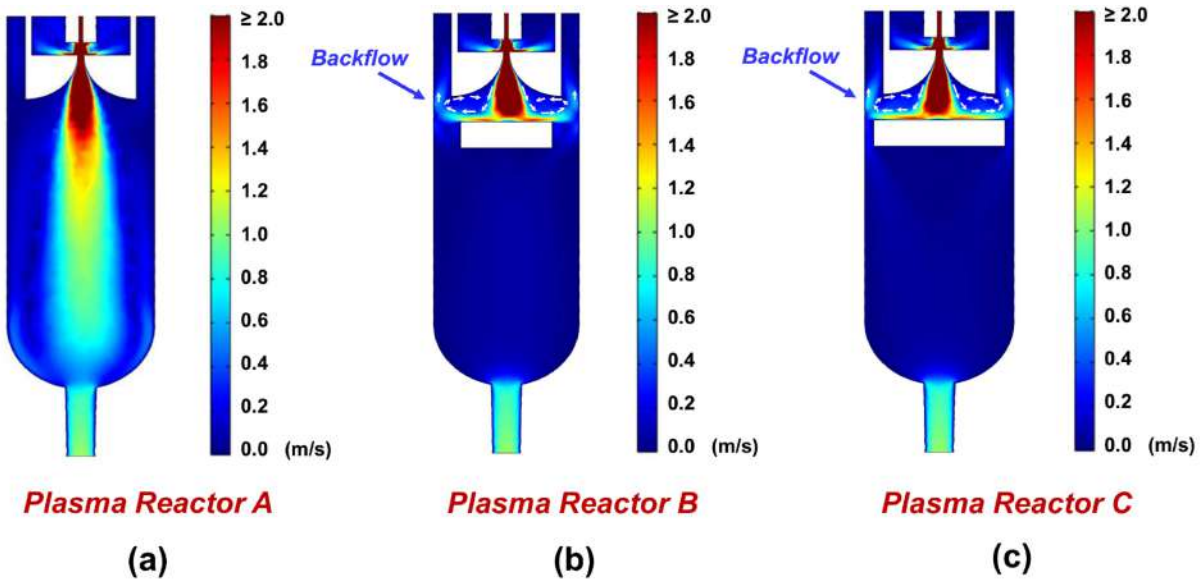

Fig. 3 Simulated contours of gas velocity magnitude on the cross-section of each reactor ($Q_{(CO2\ inlet)}$ = 4 L/min, D = 10mm).

To get insights into the effect of the tray on the gas flow field, the gas flow field and gas velocity in the gliding arc reactor has been simulated using COMSOL Multiphysics software (three-dimensional laminar flow module) [43]. The contours of gas velocity magnitude on the cross-section of each reactor are presented in Fig. 3 (CO_2 flow rate = 4 L/min). As clearly seen from Figs. 3b and 3c, the addition of tray downstream the discharge gives rise to the formation of strong backflow above the top of the tray. Unreacted gas can thus partly flow back to the plasma area for further treatment, consequently enhancing the fraction of gas treated by plasma. This factor should be associated with

the facilitating effect of the tray on the CO_2 conversion reaction. Moreover, the direct contact of the plasma jet with the surface of the tray in *Reactor B* or *C* enables a horizontal extension of the plasma area (refer to Figs.4c_1, 4c_2 and Supplementary Fig. S1). In this way, more gas molecules can pass through the plasma area, and the gas treatment by plasma can be improved from another aspect. A larger tray enables a higher fraction of gas treated by plasma, explaining why it shows a better performance than the small tray at a high flow rate.

To conclude, the addition of tray downstream the discharge decreases the reaction performance at low flow rates (*i.e.*, 2 L/min for *Reactor B* and 2-4 L/min for *Reactor C*) because of the increased gas temperature, whereas remarkably enhances both the CO_2 conversion and energy efficiency at relatively high flow rates (*i.e.*, $\geq$ 3 L/min for *Reactor B* and $\geq$ 5 L/min for *Reactor C*), resulting from the improved gas treatment by plasma. The "best results" appear to be obtained in *Reactor C*, with a CO_2 flow rate of 7 L/min, yielding a CO_2 conversion of 8.5% and energy efficiency of 34.3%. Interestingly, the energy efficiency in this modified gliding arc reactor is significantly higher compared with that in typical DBD and corona discharges (<10%) [6]. Note that similar results can be obtained as well in a three-dimensional gliding arc plasmatron reactor with reverse vortex flow configuration [5, 33]. The modified reactor by adding a tray and the plasmatron with vortex flow can both improve the fraction of gas passing through the arc and thus show better performance than a classical gliding arc. Whereas, *Reactor C* cannot provide excellent performance in a wide range of flow rates and the relatively high gas temperature in the plasma area is also unfavourable from the operation point of view. Therefore, *Reactor B* was further used to investigate the effect of combining plasma with the commonly used photocatalyst TiO_2 on the CO_2 dissociation reaction.

3.2 Effect of in-plasma catalysis

TiO_2 has been proved to have synergistic effect with non-thermal plasma in various applications, such as NO_x reduction [44], VOCs degradation (*e.g.*, toluene, benzene and naphthalene) [45], organic wastewater treatment [46], or even *p*-nitrophenol contaminated soil remediation [47], but not yet applied in gliding arc for CO_2 activation. In the experiments, by adjusting the position of the catalyst bed, the vertical distance between the electrode tip and the catalyst surface (D) varied in the range of 5, 10, 15, 20 mm, yielding two combination modes of plasma and catalysis, *i.e.*, in-plasma catalysis (D = 5, 10 mm) and post-plasma catalysis (D = 15, 20 mm). The results for the in-plasma catalysis mode with different positions of the catalyst beds are illustrated in Fig. 4. The photos were taken by a digital single-lens reflex camera with an exposure time of 1/100s and aperture of F10.

As shown in Figs. $4c_1$ and $4c_2$, in this mode the gliding arc plasma jet can be in direct contact with the catalyst surface, yielding an interaction between plasma and catalyst. Results with the presence of catalysts at relatively high flow rates ($\geq$ 5 L/min for D = 5 mm and $\geq$ 6 L/min for D = 10 mm) were not plotted, because during experiments the catalyst particles were readily blown out of the catalyst bed due to the high-speed gas flow. It is observed that the combination of TiO_2 catalysts with the discharge drastically improves both the conversion of CO_2 and energy efficiency of the process.

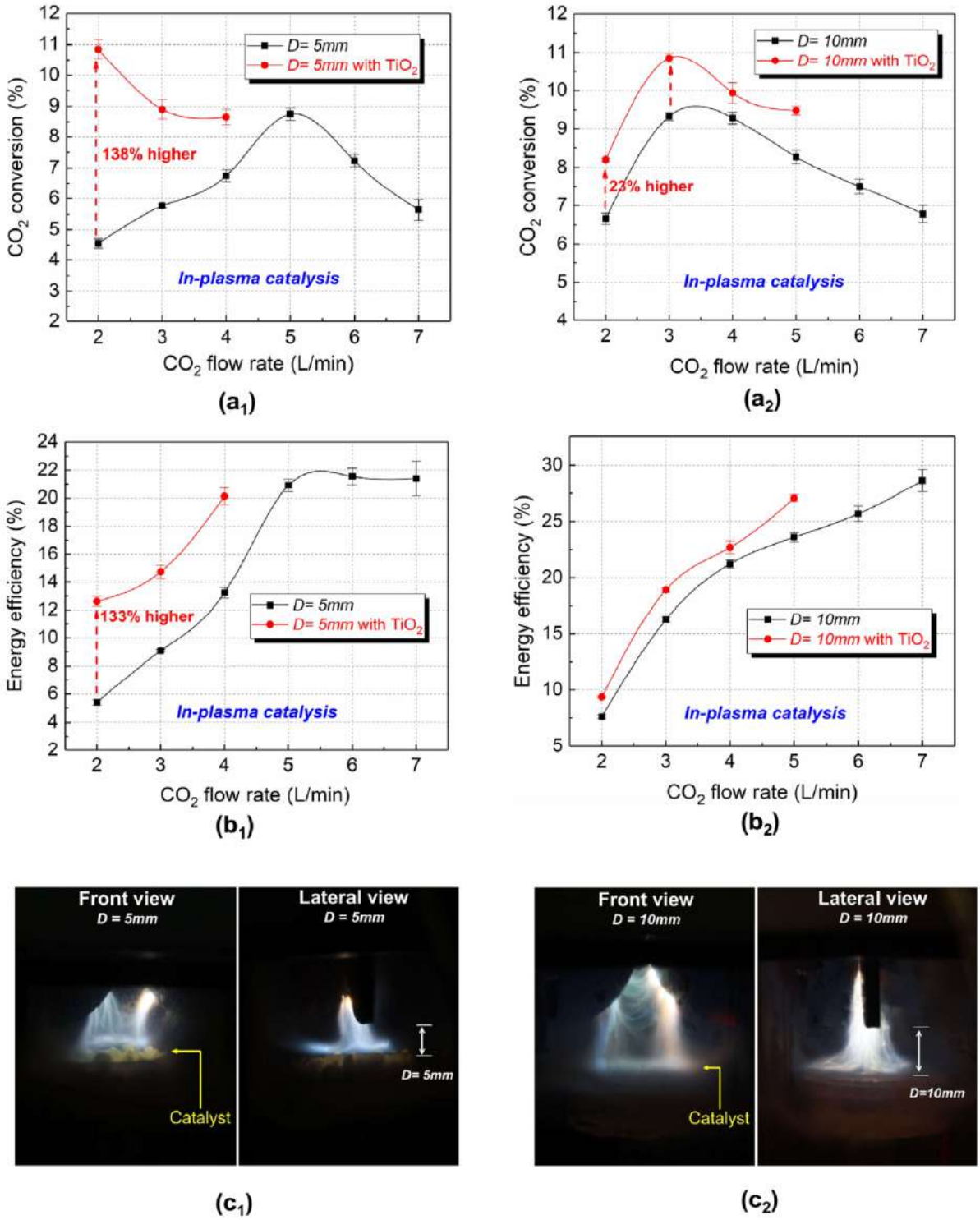

Fig. 4. Effect of in-plasma catalysis on the CO_2 conversion and energy efficiency with different positions of the catalyst bed (a_1, b_1, c_1 for D = 5 mm, a_2, b_2, c_2 for D = 10 mm; *Reactor B*).

Specifically, a shorter distance between the electrodes and catalysts at relatively low flow rates

exhibits exceptional performance. For instance, in the reactor with D = 5 mm at a flow rate of 2 L/min (Figs. 4a_1 and 4b_1), the integration of TiO_2 catalysts with plasma dramatically enhances the CO_2 conversion by 138% (from 4.6% to 10.8%) and the energy efficiency by 133% (from 5.4% to 12.6%). Rising flow rate from 2 to 4 L/min leads to a drop of the CO_2 conversion from 10.8% to 8.7% in this case, probably resulting from the reduced retention time of the reactive CO_2 plasma on the catalyst surface. Interestingly, although the reactor with D = 5 mm at a flow rate of 2 L/min shows the highest gas temperature (see Supplementary Table S2), it yields the best results when the catalyst is present, indicating that the negative effect of higher temperature, in this case, is more than compensated by the positive effect of plasma activation of the catalyst.

For the reactor with D = 10 mm in Figs. 4a_2 and 4b_2, the reaction performance also shows notable enhancement with the addition of TiO_2 catalyst, but less pronouncedly in comparison to the reactor with D = 5 mm. The CO_2 conversion shows an increase of 23% at a flow rate of 2 L/min in comparison to the single plasma process and reaches the maximum value of 10.9% at a flow rate of 3 L/min. Upon rising flow rate, both the conversion of CO_2 and energy efficiency, in this case, have similar variation profiles with that in the absence of a catalyst. These results suggest the formation of a significant synergistic effect in the conversion of CO_2 when combining gliding arc plasma with TiO_2 photocatalysts.

3.3 Effect of post-plasma catalysis

Fig. 5 exhibits the effect of the post-plasma catalysis (two-stage plasma catalysis) with D = 15 and 20 mm on the conversion of CO_2. In this mode, no direct contact between the plasma jet and the catalyst surface occurs (see Figs. 4c_1 and 4c_2).

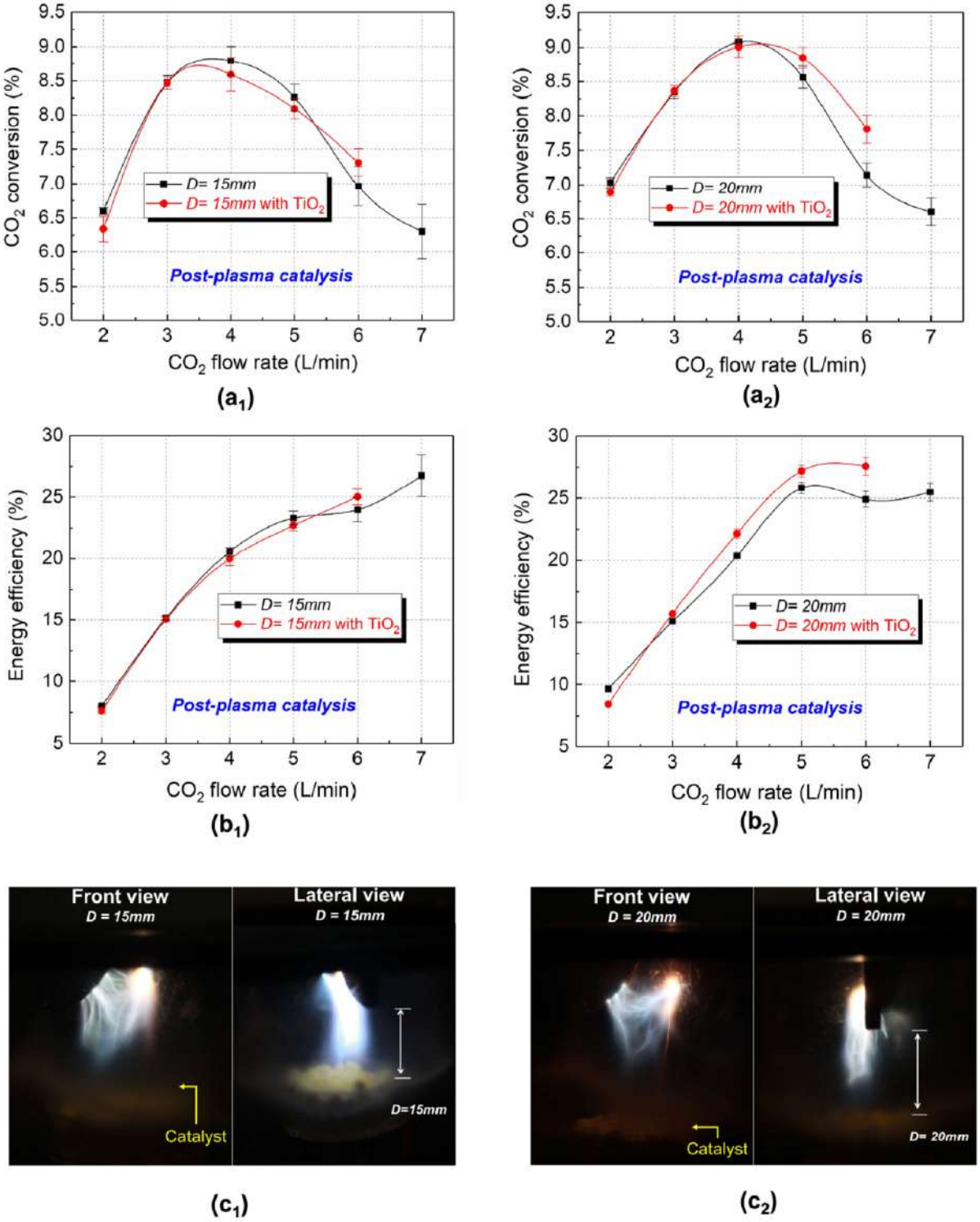

Fig. 5 Effect of post-plasma catalysis on the CO_2 conversion and energy efficiency with different positions of the catalyst bed (a_1, b_1, c_1 for D = 15 mm, a_2, b_2, c_2 for D = 20 mm; *Reactor B*).

In comparison to the in-plasma catalysis mode, the post-plasma catalysis exhibits a negligible

effect on the CO_2 conversion reaction, as seen from the various profiles of the CO_2 conversion and energy efficiency in Fig. 5. In a post-plasma catalysis configuration, only long-life species produced in plasma that can touch the catalyst surface could affect the catalyst activity [48, 49]. This is probably the reason why a slight improvement of the CO_2 conversion and energy efficiency can be observed with relatively high flow rate (6 L/min for D = 15 mm and ≥ 5 L/min for D = 20 mm).

The above results allow us to conclude that the synergy of gliding arc plasma with TiO_2 for CO_2 activation can form only in the in-plasma catalysis mode.

It is also interesting to note that varying the position of the tray (without catalyst) from D = 10 mm to 20 mm has no remarkable influence on the reaction performance, as indicated from the comparison among Figs. $4a_2$, $4b_2$ and Figs. $5a_1$, $5b_1$, $5a_2$, $5b_2$. Whereas, the reactor with D = 5 mm exhibits a relatively lower CO_2 conversion and energy efficiency (see Figs. $4a_1$, $4b_1$), probably resulting from the higher gas temperature in the plasma area (see Supplementary Table S2) that may induce the reverse reaction of CO_2 dissociation. Further study of plasma modelling will be carried out to confirm this hypothesis.

4. Discussion

Based on the measurement results by using a thermal infrared imager, the temperature of the catalyst surface in the discharge is in the range of 219 to 650 ^oC under the studied conditions. To elucidate whether the heating effect of gliding arc plasma plays a role in activating the catalyst, blank experiments in the absence of plasma were performed by heating the reactor gradually from 100 to 1000 ^oC (higher than the catalyst surface temperature in the presence of plasma), and no conversion of

CO_2 was observed, indicating that the activation of TiO_2 catalysts in the gliding arc plasma is not related to the thermocatalytic mechanisms.

It is well known that as a photocatalyst TiO_2 can be activated when absorbing photon energy (hv) that is greater than or equal to the band gap energy (3.0 eV for rutile phase and 3.2 eV for anatase phase) between the valence band (VB) and the conductive band (CB) to form the electron-hole pairs (e^- - h^+) [14, 50]. Although it is a fact that non-thermal CO_2 plasma can generate UV radiation [14, 18], its photon flux is too low to make any significant contribution to the activation of TiO_2 catalysts, as widely reported and demonstrated in various works [14, 41, 48]. For instance, in an atmospheric air-surface discharge by Sano *et al*., the total UV intensity was only 2.5 μW/cm^2 when the input power was 5W, generating relatively weak photocatalysis effect with a contribution of less than 0.2% against the acetaldehyde decomposition by the plasma itself [51].

In a DBD plasma, Mei *et al.* confirmed the significance of the physical effect, *i.e.*, enhancement of the electric field that was induced by packing TiO_2 pellets into the discharge gap, activating the photocatalytic reactions for CO_2 dissociation [14]. Whereas, in this work, the physical effect of adding TiO_2 particles into the catalyst tray is thought to be negligible as the catalyst tray was placed downstream the discharge gap. In addition, the flow field inside the reactor is hardly affected by the addition of TiO_2 particles since quartz pellets with similar size were placed in the tray for the comparative experiments without catalysts. It is also interesting to note that stone and glass bead with similar size with that of the TiO_2 were also used to perform comparative experiments, and no perceptible improvement of the CO_2 conversion performance was observed.

We can conclude that the gliding arc plasma-activated photocatalytic reaction is considered as the

dominant contributor to the synergistic effect of plasma and catalysis for CO_2 activation. As proposed by Whitehead et al. [49, 52], in a plasma catalysis system, the electrons existing in discharge with an electron energy of > 3.0 eV can create e^- - h^+ pairs on the rutile TiO_2 surface (Eq. (5)), like the effect of UV excitation. The production of e^- - h^+ pairs, which facilitates the further redox reaction, is considered as the initial and critical step of photocatalytic reactions.

$$TiO_2 + e^- \left(> 3.0 \text{ eV} \right) \rightarrow h^+ + e^- \quad (5)$$

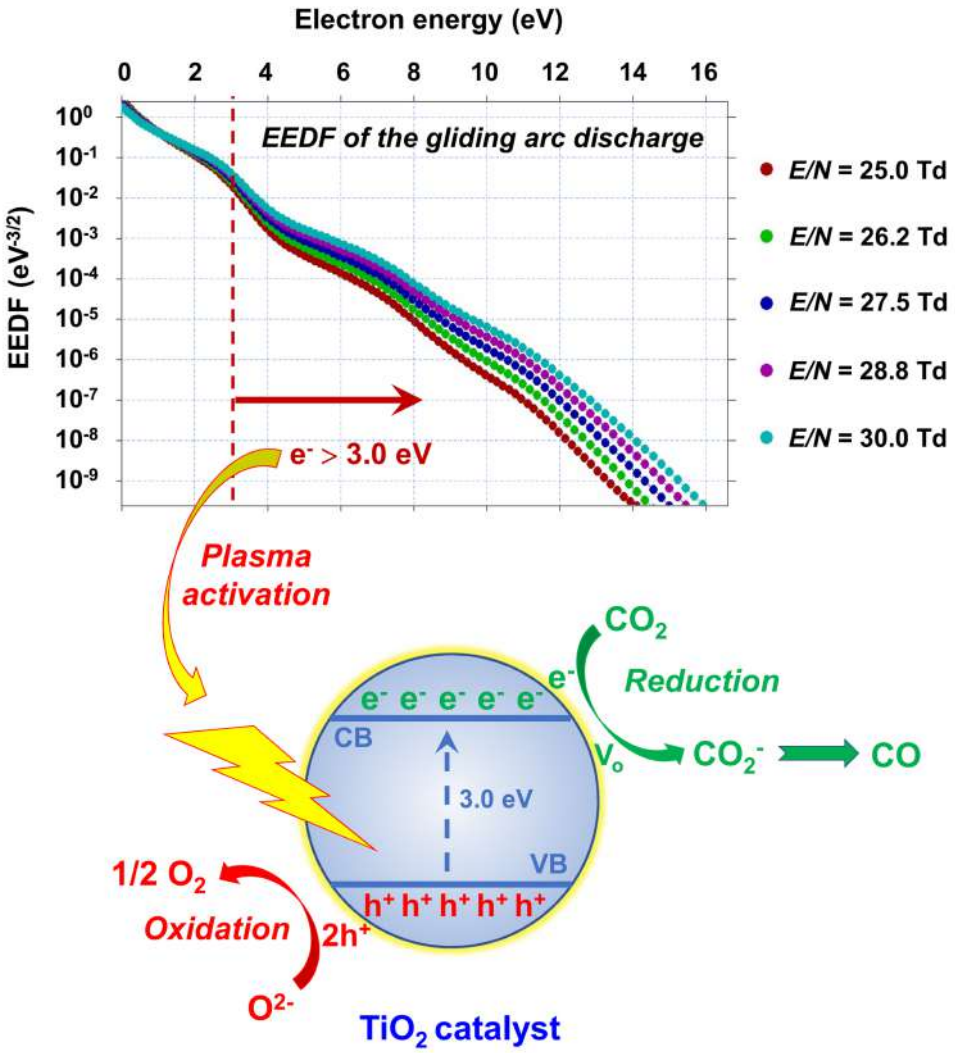

Fig. 6 EEDF of the gliding arc discharge and the possible reaction mechanisms of the plasma photocatalytic CO_2 dissociation process.

To get insight into the energy level of the electrons generated by the CO_2 gliding arc plasma, the electron energy distribution function (EEDF) was calculated by solving the Boltzmann equation using a commonly used solver, *i.e.*, BOLSIG+ [10, 19, 53]. The cross-section data needed for various collisional processes in CO_2 were derived from Ref. [54]. Based on the electrical signals obtained by the oscilloscope, the reduced electric field (*E/N*, *E* is the electric field intensity, and *N* is the total gas-particle number density) under the studied conditions is in the range of 25-30 Td. The results for the EEDF are plotted in Fig. 6 (upper figure), yielding estimated mean electron energy of 1.0-1.2 eV, which is inconsistent with previous works [19, 55]. Although the mean electron energy is relatively low, the high-energy tail of the EEDF suggests the existence of energetic electrons in the CO_2 gliding arc plasma at energies exceeding the activation threshold (3.0 eV). In addition, gliding arc plasma has a relatively high electron density (*e.g.*, 10^{13}-10^{14} cm^{-3}) [19, 55], providing significant numbers of energetic electrons for the activation of e^- - h^+ pairs on the TiO_2 surface.

However, the e^- - h^+ pairs are ready to be recombined with the fast rate (~10^{-9}s), limiting the efficiency of CO_2 conversion [56, 57]. In this regard, the defect disorders in photocatalyst, like oxygen vacancy (V_o), can contribute significantly to the CO_2 reduction processes by providing active sites for the adsorption and thus activation of CO_2 [7, 14, 41, 58]. To understand the surface structure of the TiO_2, XPS measurement was performed, and the deconvolution spectra of Ti 2p are plotted in Fig. 7. The XPS spectra suggest the existence of both the formal valence Ti^{4+} and Ti^{3+} states on the catalyst surface. The appearance of the Ti^{3+} state indicats the generation of V_o on the TiO_2 surface due to the reaction Eq. (6) [59].

$$2Ti^{4+} + O^{2-} \rightarrow V_o + 2Ti^{3+} + 1/2O_2 \quad (6)$$

, where O^{2-} is the lattice oxygen.

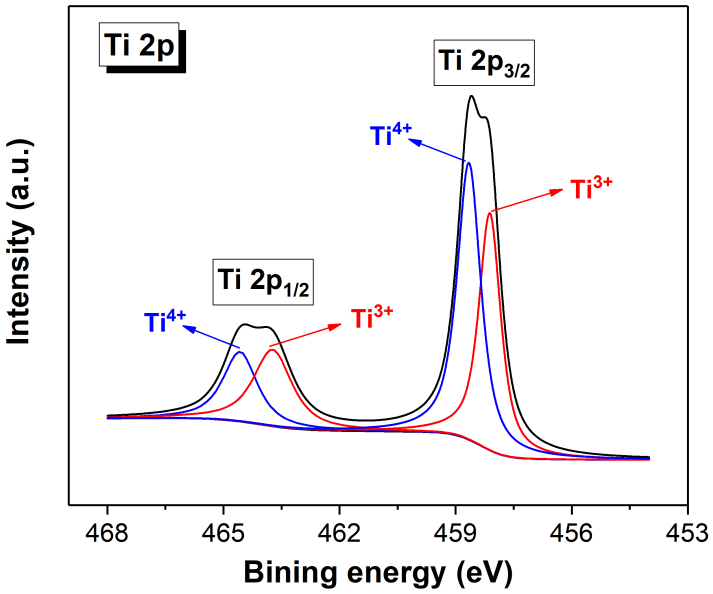

Fig. 7 XPS spectra of Ti 2p peaks of TiO_2.

It has been widely reported and investigated that, the presence of V_o on the rutile (110) facet (the dominant facet of rutile TiO_2, see the XRD patterns in Supplementary Fig. S2) can significantly induce the formation of new stable adsorption structures with an enhanced activation of the C–O bonds [56, 60-62]. Reasonable mechanisms of the gliding arc plasma photocatalytic CO_2 activation process are schematically given in Fig. 6. After the activation of e^- - h^+ pairs by the energetic electrons in plasma, the CB electrons (e^-) formed can be transferred spontaneously to the absorbed CO_2 molecules in the V_o, leading to the formation of CO_2^- anion (Eq. (4)) [7, 14, 56, 57]. CO_2^- can then dissociate into CO with the occupation of an oxygen atom into the V_o [7, 56]. The above two processes yield an overall reaction of Eq. (5). Note that this dissociative electron attachment process of CO_2 proceeds more readily for the absorbed CO_2 in the V_o than for the CO_2 in gas phase due to its low threshold energy (1.4 eV versus 5-10 eV) [7, 62]. The release of O_2 results from the oxidizing reaction of the lattice O^{2-} anions with h^+ (Eq. (6)), in which process V_o can be regenerated [14]. The electron attachment of Ti^{4+}

to produce Ti^{3+} also happens to balance the charge (Eq. (10)) [14].

$$CO_2 + e^- \rightarrow CO_2^- \quad (7)$$

$$CO_2 + [TiO_2 + V_o] \rightarrow CO + [TiO_2] \quad (8)$$

$$2h^+ + O^{2-} \rightarrow 1/2\ O_2 \quad (9)$$

$$e^- + Ti^{4+} \rightarrow Ti^{3+} \quad (10)$$

Note that the combination of Eqs. (9) and (10) yields an overall reaction of Eq. (6).

The above-proposed plasma activation mechanisms were further confirmed by the negligible influence of the post-plasma catalysis on the activation of CO_2 because the short-life electrons in plasma cannot touch and activate the catalyst surface.

It is also interesting to note that in this work both anatase TiO_2 and rutile TiO_2 catalysts have been investigated for plasma catalytic CO_2 activation, but only the TiO_2 catalyst with rutile phase showed facilitating effect on the reaction performance.

5. Conclusions

In summary, plasma-TiO_2 catalytic activation of CO_2 has been investigated in a modified gliding arc reactor. The addition of a tray downstream the discharge can improve the fraction of gas treated by plasma due to the formation of strong backflow above the top of the tray and the horizontal extension of the plasma area. The integration of TiO_2 catalysts with gliding arc plasma in the in-plasma catalysis mode formed an exceptionally synergistic effect, which dramatically enhanced the CO_2 conversion by 138% (from 4.6% to 10.8%) and the energy efficiency by 133% (from 5.4% to 12.6%) at a flow rate of 2 L/min. The existence of energetic electrons at energies exceeding the activation threshold of TiO_2

photocatalyst (3.0 eV) is considered as the primary contributor to the synergy of gliding arc plasma with TiO_2 photocatalyst by motivating the activation of electron-hole pairs on the catalyst surface. The presence of oxygen vacancy (V_o) on the TiO_2 surface is vital in facilitating the adsorption and thus activation of CO_2 molecules. This work provides critical clues for further enhancement of CO_2 activation in the promising gliding arc discharge reactor by plasma catalysis.

References

[1]. Sharma RK, Gaur R, Yadav M, et al. An efficient copper-based magnetic nanocatalyst for the fixation of carbon dioxide at atmospheric pressure. Sci Rep. 2018;8(1):1901.

[2]. USEPA E. Inventory of US greenhouse gas emissions and sinks: 1990–2013. Washington, DC, USA, EPA. 2015.

[3]. Division ESRLGM. A Global Network for Measurements of Greenhouse Gases in the Atmosphere. 2018.

[4]. Chen G, Georgieva V, Godfroid T, et al. Plasma assisted catalytic decomposition of CO_2. Appl Catal B. 2016;190:115-24.

[5]. Ramakers M, Trenchev G, Heijkers S, et al. Gliding Arc Plasmatron: providing an alternative method for carbon dioxide conversion. Chem Sus Chem. 2017;10(12):2642-52.

[6]. Snoeckx R, Bogaerts A. Plasma technology–a novel solution for CO_2 conversion? Chem Soc Rev. 2017;46(19):5805-63.

[7]. Chen G, Godfroid T, Britun N, et al. Plasma-catalytic conversion of CO_2 and CO_2/H_2O in a surface-wave sustained microwave discharge. Appl Catal B. 2017;214:114-25.

[8]. Li L, Zhang H, Li XD, et al. Plasma-assisted CO_2 conversion in a gliding arc discharge: Improving performance by optimizing the reactor design. J CO_2 Util. 2019;29:296-303.

[9]. Mei D, Zhu X, He YL, et al. Plasma-assisted conversion of CO_2 in a dielectric barrier discharge reactor: understanding the effect of packing materials. Plasma Sources Sci T. 2014;24(1):015011.

[10]. Wang W, Berthelot A, Kolev S, Tu X, Bogaerts A. CO_2 conversion in a gliding arc plasma: 1D cylindrical discharge model. Plasma Sources Sci T. 2016;25(6):065012.

[11]. Mei D, Tu X. Conversion of CO_2 in a cylindrical dielectric barrier discharge reactor: Effects of plasma processing parameters and reactor design. J CO_2 Util. 2017;19:68-78.

[12]. Zhang H, Li L, Li XD, et al. Warm plasma activation of CO_2 in a rotating gliding arc discharge reactor. J CO_2 Util. 2018;27:472-9.

[13]. Paulussen S, Verheyde B, Tu X, et al. Conversion of carbon dioxide to value-added chemicals in atmospheric pressure dielectric barrier discharges. Plasma Sources Sci T. 2010;19(3):034015.

[14]. Mei D, Zhu X, Wu C, et al. Plasma-photocatalytic conversion of CO_2 at low temperatures: Understanding the synergistic effect of plasma-catalysis. Appl Catal B. 2016;182:525-32.

[15]. Fridman A. Plasma chemistry: Cambridge university press; 2008.

[16]. Liu S, Mei D, Wang L, et al. Steam reforming of toluene as biomass tar model compound in a gliding arc discharge reactor. Chem Eng J. 2017;307:793-802.

[17]. Zhang H, Wang W, Li X, et al. Plasma activation of methane for hydrogen production in a N_2 rotating gliding arc warm plasma: A chemical kinetics study. Chem Eng J. 2018;345:67-78.

[18]. Zhang H, Li X, Zhu F, et al. Plasma assisted dry reforming of methanol for clean syngas production and high-efficiency CO_2 conversion. Chem Eng J. 2017;310:114-9.

[19]. Zhang H, Du C, Wu A, et al. Rotating gliding arc assisted methane decomposition in nitrogen for hydrogen production. Int J Hydrogen Energ. 2014;39(24):12620-35.

[20]. Gao Y, Zhang S, Sun H, et al. Highly efficient conversion of methane using microsecond and nanosecond pulsed spark discharges. Appl Energ. 2018;226:534-45.

[21]. Ozkan A, Bogaerts A, Reniers F. Routes to increase the conversion and the energy efficiency in the splitting of CO_2 by a dielectric barrier discharge. J Phys D Appl Phys. 2017;50(8):084004.

[22]. Snoeckx R, Heijkers S, Van Wesenbeeck K, et al. CO_2 conversion in a dielectric barrier discharge plasma: N_2 in the mix as a helping hand or problematic impurity? Energ Environ Sci. 2016;9(3):999-1011.

[23]. Mei D, Tu X. Atmospheric Pressure Non- Thermal Plasma Activation of CO_2 in a Packed- Bed Dielectric Barrier Discharge Reactor. Chem Phys Chem. 2017;18(22):3253-9.
[24]. Van Laer K, Bogaerts A. Improving the Conversion and Energy Efficiency of Carbon Dioxide Splitting in a Zirconia-Packed Dielectric Barrier Discharge Reactor. Energ Technol. 2015;3(10):1038-44.
[25]. Xu S, Whitehead JC, Martin PA. CO_2 conversion in a non-thermal, barium titanate packed bed plasma reactor: The effect of dilution by Ar and N_2. Chem Eng J. 2017;327:764-73.
[26]. Ozkan A, Dufour T, Silva T, et al. The influence of power and frequency on the filamentary behavior of a flowing DBD—application to the splitting of CO_2. Plasma Sources Sci T. 2016;25(2):025013.
[27]. Alliati M, Mei DH, Tu X. Plasma activation of CO_2 in a dielectric barrier discharge: A chemical kinetic model om the microdischarge to the reactor scales. J CO_2 Utili. 2018;In press.
[28]. Van RG, Van BD, Harder N, et al. Taming microwave plasma to beat thermodynamics in CO2 dissociation. Faraday Discuss. 2015;183:233-48.
[29]. Spencer L, Gallimore A. CO_2 dissociation in an atmospheric pressure plasma/catalyst system: a study of efficiency. Plasma Sources Sci T. 2012;22(1):015019.
[30]. Xu W, Li MW, Xu GH, et al. Decomposition of CO_2 using DC corona discharge at atmospheric pressure. Jpn J Appl Phys. 2004;43(12R):8310.
[31]. Bongers W, Bouwmeester H, Wolf B, et al. Plasma- driven dissociation of CO_2 for fuel synthesis. Plasma Process Polym. 2017;14(6):1600126.
[32]. Sun S, Wang H, Mei D, et al. CO_2 conversion in a gliding arc plasma: Performance improvement based on chemical reaction modeling. J CO_2 Util. 2017;17:220-34.
[33]. Nunnally T, Gutsol K, Rabinovich A, et al. Dissociation of CO_2 in a low current gliding arc plasmatron. J Phys D Appl Phys. 2011;44(27):274009.
[34]. Li L, Zhang H, Li X, et al. Plasma-assisted CO_2 conversion in a gliding arc discharge: Improving performance by optimizing the reactor design. J CO_2 Util. 2019;29: 296-303.
[35]. Wang W, Mei D, Tu X, et al. Gliding arc plasma for CO_2 conversion: Better insights by a combined experimental and modelling approach. Chem Eng J. 2017;330:11-25.
[36]. Berthelot A, Bogaerts A. Modeling of CO_2 splitting in a microwave plasma: how to improve the conversion and energy efficiency. J Phys Chem C. 2017;121(15):8236-51.
[37]. Zhang H, Zhu F, Li X, et al. Steam reforming of toluene and naphthalene as tar surrogate in a gliding arc discharge reactor. J Hazard Mater. 2019;369:244-53.
[38]. Fridman A, Nester S, Kennedy LA, et al. Gliding arc gas discharge. Prog Energ Combust. 1999;25(2):211-31.
[39]. Chen HL, Lee HM, Chen SH, et al. Review of plasma catalysis on hydrocarbon reforming for hydrogen production—interaction, integration, and prospects. Appl Catal B. 2008;85(1-2):1-9.
[40]. Whitehead JC. Plasma–catalysis: the known knowns, the known unknowns and the unknown unknowns. J Phy D Appl Phys. 2016;49(24):243001.
[41]. Chen G, Britun N, Godfroid T, et al. An overview of CO_2 conversion in a microwave discharge: the role of plasma-catalysis. J Phy D Appl Phys. 2017;50(8):084001.
[42]. Tsang W, Hampson R. Chemical kinetic data base for combustion chemistry. Part I. Methane and related compounds. J Phys Chem Ref Data. 1986;15(3):1087-279.
[43]. Multiphysics C. v. 5.2. COMSOL AB, Stockholm, Sweden. 2015.
[44]. Daito S, Tochikubo F, Watanabe T. NOx removal process in pulsed corona discharge combined with TiO_2 photocatalyst. Jpn J Appl Phys. 2001;40(4R):2475.
[45]. Kang M, Kim B-J, Cho SM, et al. Decomposition of toluene using an atmospheric pressure plasma/TiO_2 catalytic system. J Mol Catal A Chem. 2002;180(1-2):125-32.

[46]. Ghezzar M, Abdelmalek F, Belhadj M, et al. Enhancement of the bleaching and degradation of textile wastewaters by Gliding arc discharge plasma in the presence of TiO_2 catalyst. J Hazard Mater. 2009;164(2-3):1266-74.
[47]. Wang TC, Lu N, Li J, et al. Plasma-TiO_2 catalytic method for high-efficiency remediation of p-nitrophenol contaminated soil in pulsed discharge. Env Sci T. 2011;45(21):9301-7.
[48]. Wu Z, Zhu Z, Hao X, et al. Enhanced oxidation of naphthalene using plasma activation of TiO_2/diatomite catalyst. J Hazard Mater. 2018;347:48-57.
[49]. Wallis AE, Whitehead JC, Zhang K. Plasma-assisted catalysis for the destruction of CFC-12 in atmospheric pressure gas streams using TiO_2. Catal Lett. 2007;113(1-2):29-33.
[50]. Cao YQ, Zhao XR, Chen J, et al. TiO_xN_y Modified TiO_2 Powders Prepared by Plasma Enhanced Atomic Layer Deposition for Highly Visible Light Photocatalysis. Sci Rep. 2018;8(1):12131.
[51]. Sano T, Negishi N, Sakai E, et al. Contributions of photocatalytic/catalytic activities of TiO_2 and γ-Al_2O_3 in nonthermal plasma on oxidation of acetaldehyde and CO. J Mol Catal A Chem. 2006;245(1):235-41.
[52]. Whitehead JC. Plasma catalysis: A solution for environmental problems. Pure Appl Chem. 2010;82(6):1329-36.
[53]. Hagelaar G, Pitchford L. Solving the Boltzmann equation to obtain electron transport coefficients and rate coefficients for fluid models. Plasma Sources Sci T. 2005;14(4):722.
[54]. MORGAN database, http://www.lxcat.laplace.univ-tlse.fr [Internet]. retrieved June 4, 2013.
[55]. Nunnally TP. Application of low current gliding arc plasma discharges for hydrogen sulfide decomposition and carbon dioxide emission reduction. 2011.
[56]. Liu L, Li Y. Understanding the reaction mechanism of photocatalytic reduction of CO_2 with H_2O on TiO_2-based photocatalysts: a review. Aerosol Air Qual Res. 2014;14(2):453-69.
[57]. Nahar S, Zain M, Kadhum AAH, et al. Advances in photocatalytic CO_2 reduction with water: a review. Mater. 2017;10(6):629.
[58]. Huygh S, Bogaerts A, Neyts EC. How oxygen vacancies activate CO_2 dissociation on TiO_2 anatase (001). J Phys Chem C. 2016;120(38):21659-69.
[59]. Liu L, Zhao C, Li Y. Spontaneous dissociation of CO_2 to CO on defective surface of Cu (I)/TiO_2–x nanoparticles at room temperature. J Phys Chem C. 2012;116(14):7904-12.
[60]. Acharya D, Camillone III N, Sutter P. CO_2 Adsorption, Diffusion, and Electron-Induced Chemistry on Rutile TiO2 (110): A Low-Temperature Scanning Tunneling Microscopy Study. J Phys Chem C. 2011;115(24):12095-105.
[61]. Tan S, Zhao Y, Zhao J, Wang Z, Ma C, Zhao A, et al. CO_2 dissociation activated through electron attachment on the reduced rutile TiO_2 (110)-1× 1 surface. Phys Rev B. 2011;84(15):155418.
[62]. Lee J, Sorescu DC, Deng X. Electron-induced dissociation of CO_2 on TiO_2 (110). J Am Chem Soc. 2011;133(26):10066-9.

Acknowledgements

The authors acknowledge the financial support from the National Natural Science Foundation of China (No. 51706204), National Key Technologies R&D Program (No. YS2018YFE010498) and the European Union's Horizon 2020 research and innovation programme under the Marie Skłodowska-

Curie grant agreement No 823745. XT and NW thank the financial support from the State Key Laboratory of Electrical Insulation and Power Equipment at Xi'an Jiaotong University (No. EIPE19207).

Competing interests

The authors declare no competing interests.